Rapid flow of dry granular materials down inclined chutes impinging on rigid walls

Shiva P. Pudasaini[a)]
Faculty of Civil Engineering and Geodesy, Institute and Laboratory of Geotechnics, Darmstadt University of Technology, Petersenstrasse 13, D-64287 Darmstadt, Germany

Kolumban Hutter
Bergstrasse 5, CH-8044 Zürich, Switzerland

Shu-San Hsiau and Shih-Chang Tai
Department of Mechanical Engineering, National Central University, No. 300 Jung-da Road, Chung-Li 32054, Taiwan

Yongqi Wang
Institute of Geotechnical Engineering, University of Natural Resources and Applied Life Sciences (BOKU), Feismantelstrasse 4, A-1180 Vienna, Austria

Rolf Katzenbach
Faculty of Civil Engineering and Geodesy, Institute and Laboratory of Geotechnics, Darmstadt University of Technology, Petersenstrasse 13, D-64287 Darmstadt, Germany

(Received 12 September 2006; accepted 30 January 2007; published online 30 May 2007)

We performed laboratory experiments of dry granular chute flows impinging an obstructing wall. The chute consists of a 10 cm wide rectangular channel, inclined by 50° relative to the horizontal, which, 2 m downslope abruptly changes into a horizontal channel of the same width. 15 l of quartz chips are released through a gate with the same width as the chute and a gap of 6 cm height, respectively. Experiments are conducted for two positions of the obstructing wall, (i) 2 m below the exit gate and perpendicular to the inclined chute, and (ii) 0.63 m into the horizontal runout and then vertically oriented. Granular material is continuously released by opening the shutter of the silo. The material then moves rapidly down the chute and impinges on the obstructing wall. This leads to a sudden change in the flow regime from a fast moving supercritical thin layer to a stagnant thick heap with variable thickness and a surface dictated by the angle of repose typical for the material. We conducted particle image velocimetry (PIV) experiments by recording the moving material from the side with charge coupled devices (CCD) cameras. The experiment was also video recorded. From the CCD data velocities were also deduced using the PIV technique. In order to compare the results here we describe the experiments for the same material and the same gap width of the silo gate but for the two positions of the obstructing wall. Analysis of the shock front formation and propagation upslope, evolution of the height of the supercritical flow, impact velocity and momentum are presented and discussed in detail. Computed and derived shock front heights match well.
 [DOI: 10.1063/1.2726885]

I. INTRODUCTION

The flow of the debris avalanche is characterized by three different regimes: (i) the starting zone where rupture and fragmentation of the solid material occurs, (ii) the avalanching zone where the granular material reaches fast supercritical speed, and (iii) the runout zone where the moving mass is decelerated and comes to a rather sudden standstill. In this paper we are concerned with the experiments on the runout zone. Observations in the laboratory and in nature show that the rapid flow regime is characterized by more or less uniform velocity profiles with depth and dominant sliding at the base, while in the deposition regime and, in particular, in the transition region from the rapid flow into the deposition zone shock-like structures form, and an overall depth flow changes into a surface boundary layer flow, which, further downstream, quickly slows down and eventually settles. So, whereas the flow state in the rapid flow regime of the avalanche is reasonably approximated by a depth integrated dynamical model, an adequate treatment of the deposition regime and the regions in the vicinity of an obstacle requires better resolution without the reduction of the dimension.

A first step towards modelling such complicated three-dimensional flows is to reduce it to two dimensions by studying the chute flow variant first and then obtain detailed experimental information on velocities and build up of deposition geometries. Moreover, computations performed with avalanche equations, such as those based on continuum dynamics approach, in rapid granular flows have shown that

[a)]Author to whom correspondence should be addressed. Present address: Department of Geodynamics and Geophysics, University of Bonn, Nussallee 8, D-53115 Bonn, Germany. Fax: +49 228 73-2508. Electronic mail: pudasaini@geo.uni-bonn.de

difficulties (associated with the sudden jumps in field variables, e.g., the velocity components and the depth profile) arise when such flows encounter obstructions (see, e.g., Savage and Hutter,[1,2] Gray *et al.*,[3] Pudasaini,[4] Pudasaini and Hutter,[5,6] Pudasaini *et al.*,[7–9] Wang *et al.*,[10] Hutter *et al.*,[11] Denlinger and Iverson,[12] Iverson *et al.*,[13] Patra *et al.*,[14] and Pitman *et al.*[15]). Particularly notorious are configurations in which rapidly moving material impinges a wall perpendicular to the bed. In such a case, some of the material comes to a complete standstill. It was decided to study this situation in a plane flow configuration. A first step towards this end is to conduct experiments to improve our understanding of the flow.

Laboratory experiments were conducted of dry granular chute flows impinging an obstructing wall. A 10 cm wide chute was built, which consists of a straight 2 m long part and abruptly merges into the horizontal with horizontal length of 0.63 m. At the upper end this chute can be filled with a granular material of finite volume—in our case 15 l. A gate, perpendicular to the inclined chute, can suddenly be lifted by a fixed amount—here 6 cm. The gate then frees the granular material behind the gate, which starts moving down the inclined chute. It quickly acquires large velocities and forms a rather thin layer of rapidly moving material. A certain distance downstream, either still in the inclined part of the chute or in the horizontal part, an obstructing rigid wall perpendicular to the channel is erected. The approaching material impinges on it; as a result, the flow goes through a violent transition from the thin-layered rapid flow with virtually uniform velocity profiles through the depth over a relatively short region with very large deceleration of the particles and reorientation of their flow direction. This flow persists as long as the granular flux from the upstream region continues.

In the heap that is formed the velocities are by no means uniformly distributed with depth but largely restricted to a surface boundary layer (i.e., the top layer in the heap) within and close to the granular jump transition region. Below the depth of some 3–5 particles, the heap does not appear to move. More careful scrutiny reveals that at the heap surface avalanching flows rearrange the geometry to accommodate the slope close to the angle of repose. Furthermore, despite the apparent state of rest of the heap distant from the granular jump region, the particles are often not at rest, but move erratically within the deposit, not moving large distances, but rearranging the conformation and possibly leading to some consolidation.

In what follows, we shall describe the experimental method and discuss the results of two different experiments with quartz sand particles.

II. EXPERIMENTAL APPARATUS, ARRANGEMENTS, AND CONDITIONS

Experiments were performed in a 10 cm wide chute which consisted of two straight portions, one inclined at 50°, the other horizontal. Figure 1 shows a sketch of the chute and a few construction details. Figure 2 shows a photo of the setup. Sidewalls consist of 10 mm thick transparent Plexiglas

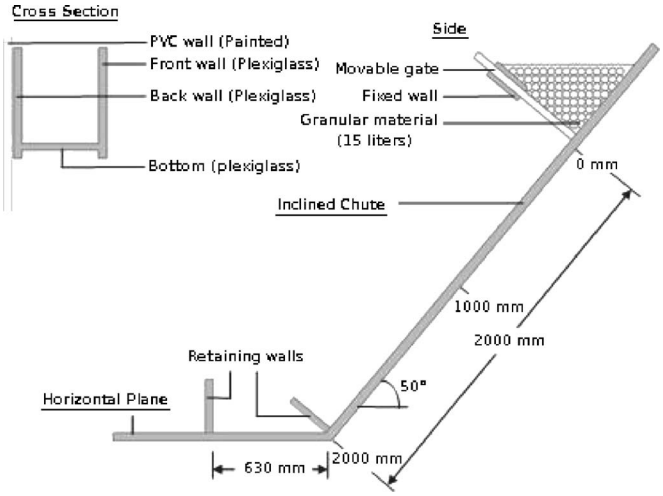

FIG. 1. Side view and cross section of the chute.

through which the moving granular mass could be photographed. The back wall, made of 10 mm thick PVC is coated and painted in black color, in order to achieve better contrast in the photographs. The basal surface is equally made of Plexiglas. All three surfaces have friction angles with our materials of about 20°–25° and lead to limited boundary layer effects. The sidewise boundary layer thickness turned out to be very thin, hardly discernible by eye, and the corresponding friction was largely ineffective (i.e., motion is approximately two-dimensional) so that the motion of the granular material could be considered to be plane; consequently, photographs of the flowing material, taken from the sides, can be considered as representative for any vertical plane within the chute. On the inclined portion of the chute, 2 m above the abrupt change into the horizontal runout, a narrow rectangular silo with a plate gate is mounted perpendicular to the channel base. The gate of the silo covers the entire 10 cm width of the chute and can be manually (but rapidly) lifted a distance not more than 10 cm. Behind this gate, dry granular material can be stored that is suddenly released upon the opening of the gate. Two positions of the retaining walls were chosen, a wall perpendicular to the

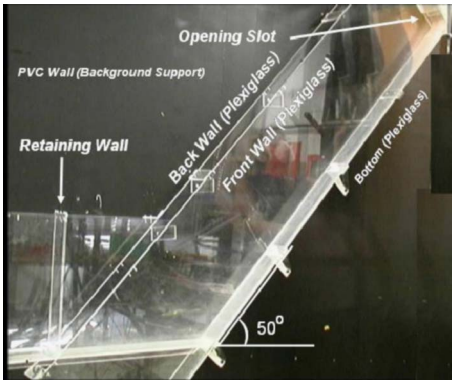

FIG. 2. (Color online) Photograph of the chute with the retaining wall in the horizontal portion of the chute.

inclined chute, 2 m below the head gate and a vertical wall, 0.63 m below the kink of the chute in the horizontal runout. We have used for our experiments 15 l of quarts chips of about 4 mm mean diameter.

In this paper, the chute that we have described is used to study the motion of dry granular material down the chute as it impinges a retaining wall that is erected at two different positions. The fast moving granular mass will, upon encountering the retaining wall, form a stagnant deposit that accumulates mass close to the wall. As the flow of mass from the reservoir continues, a shock-like transition region will move backwards from the wall, gaining mass at supercritical speed from above. Over the diffusive shock region, the flow height will increase and the velocity decrease to subcritical values and the particles come to rest as the process goes on, and the heap extends backward until the flux of granular material from above terminates.

Experiments are performed by suddenly lifting the movable gate that holds the material behind it at rest. Simultaneously with the opening of the gap that releases the material, the photographic system consisting of a video camera and one or two CCD cameras are operated for recording the motion. The video camera provides a visual impression of the motion of the layer of granular material flowing down the chute. Impinging on the upstream side of the retaining wall and accumulating material in front of it, the CCD camera takes pictures from the side perpendicular to the chute for storage in the computer system and further postprocessing of the velocity fields. Uniform illumination of the experimental region that is encountered by the flowing material is important to minimize the error in the velocities obtained by the PIV system. Detailed information on the technical peculiarities, advantages, and also the limitations of the PIV system are presented in Pudasaini,[4] Pudasaini and Hutter,[6] Pudasaini *et al.*,[9] and Eckart *et al.*[16]

Experiments were performed for fairly roundish quartz sand particles of approximately 4 mm mean diameter. The opening gap of the movable gate considered here was 6 cm and the retaining walls, stopping the granular flow, was either mounted at the end of the inclined chute, 2 m below the head gate (indicated in Fig. 2 as "opening slot," also seen in Figs. 1 and 4) or 0.63 m down into the horizontal part of the chute (see Fig. 1). The results of the two experiments are presented here.

In the experiment, the gate that extends over the entire width of the chute and holds the material in the space behind it, is suddenly removed; a gap of 6 cm is opened. This point in time ($t=0$) defines the onset of the motion of the granular material through the gate and down the chute. As it exits the opening gap, the mass accelerates down the inclined chute with decreasing height, but reaches, after some distance, almost a constant depth and therefore most likely also approximately a constant velocity condition. When the material enters the horizontal portion of the channel, it is decelerated as the flow depth is somewhat increased.

TABLE I. Experimental conditions for the two chute experiments. The mean diameter for quartz sand particles is 4 mm. The internal and bed friction angles of the material are $\phi=33°$ and $\delta=22°$, respectively. I corresponds to an inclined chute only, IH denotes the inclined chute with horizontal runout.

Expt. No.	Materials	Gap width (mm)	Chute type
3	Quartz sand	60	I
5	Quartz sand	60	IH

III. TECHNICAL DETAILS OF PARTICLE IMAGE VELOCIMETRY

The particle image velocimetry (PIV) technique is an optical measuring system which, in a granular system allows determination of particle velocities at surfaces that are directly visible to the eye and can be photographed. In our laboratory setup the particles immediately at the front Plexiglas wall can be recorded and their velocities can be deduced. The basic idea of the measuring system is as follows: The frontal boundary of the flowing granular material is illuminated twice, at times t and $t+\Delta t$. Images are captured by CCD cameras. Displacements of identifiable particles of the moving avalanche are calculated by comparing frames taken at t and $t+\Delta t$ by pattern recognition. The displacement divided by the time difference between both frames gives the velocity of the particle. We use a special PIV system (we call it a "granular PIV"), designed for nontransparent fluids, such as sand. In contrast to the usual PIV, in the granular PIV, we do not need to add any tracer particles. The surface structure of the moving and deforming granular bulk material is sufficient to determine the vector field through the cross-correlation algorithm. More detailed information on the PIV system used by us can be found in Pudasaini,[4] Pudasaini and Hutter,[6] Pudasaini *et al.*,[9] Eckart *et al.*,[16] and Tischer *et al.*[17]

The electronic and optical equipment which we use are those of the company TSI (http://www.tsi.com). This includes two CCD-cameras of type TSI PIV-CAM 13-8. The system is supplemented by wide-angle-zoom lenses of type NIKON NIKKOR AF 18–35 mm f/3.5~4.5 D IF; a synchronizer and a PC including the INSIGHT PIV-software. For illumination we used either two or four flashes (depending on either one or two cameras in use) of the type METH MECABLITZ 60 CT-4. The CCD camera has a resolution of 1280×1024 pixels and a color depth of 12 bit. Furthermore, its highest temporal resolution is four double frames per second. The time delay between the first and the second frame is set to be 1 μs. The time delay used depends on the range of the velocity gradients of the flow.

IV. EXPERIMENTAL RESULTS

We have analyzed and presented two different experiments in detail. In all experiments the chute had the dimension and arrangement as shown in Fig. 1. Table I lists the conditions in the individual runs. Data files for velocity fields measured by using PIV system and other associated plots of this paper are available at EPAPS.[18]

In this paper, we are mainly interested in understanding the transitional behavior of the granular flow from a supercritical to subcritical state. We wish to show how the "granular PIV" measurement technique can be used to study this transition, shock formation and propagation in dry and cohesionless granular flows encountering obstacles or sudden changes in the bed topography. The outcome of this study could be the basis for numerical simulation and calibration of the theoretical models both in industrial process engineering in small scale and in large scale avalanches and debris flows in steep mountain slopes. Data of this type are still lacking in the literature. With this study, we have observed that the flows are not uniform through depth in the transition zone and in the vicinity of an obstacle, rather they clearly reveal strong shear flow. In an avalanche, rock and debris flow dynamics, only two-dimensional model equations (with coordinate lines either parallel to the bottom topography fitting the slope, e.g., Pudasaini and Hutter[4,6]) or simply fixed Cartesian *xy* plane (e.g., Denlinger and Iverson[12]) are used for the predictions and hazard mappings. However, the experiments considered in this paper clearly demonstrate that, in such a transition region, there is considerable momentum transfer and velocity shearing in the direction perpendicular to the sliding surface, which cannot be neglected as in the existing models. The existing avalanche or granular flow models effectively assume uniform flow through the depth and the momentum transfer in the direction normal to the bed is thus negligible. Therefore, a fully three-dimensional model is urgently needed in order to describe the complete three-dimensional intrinsic behavior of such flows.

A. Experiment No. 3

The evolution of the pile buildup for the motion of quartz grains through the opening gate with the 6 cm gap is shown in Fig. 3. The following qualitative features are evident from the experiments for the 2 m inclined chute (Fig. 3): At the instant of first particle impingement on the retaining wall, there is violent bouncing that becomes lesser as the heap is formed. The stagnant heap in the experiments does not have constant depth; the depth is largest at the retaining wall and decreases as one moves towards the (diffusive) shock front. The shock is diffuse, i.e., the transition from the approaching supercritical flow with small height to the stagnant heap with large height is not abrupt but smooth with a characteristic *S*-shaped transition profile, whose physical characteristics are not known. In the supercritical regime above the stagnant heap, the velocity appears to be forward only, i.e., parallel to the basal surface, and there seems to be no variation of the speed with depth; plug flow seems to prevail. As the flow transits into the heap, the particle motion appears to be parallel to the *S*-shaped surface, strongly attenuated with depth and quickly coming to a standstill with increasing distance from the free surface into the heap. This boundary layer behavior is typical and may influence the local shape of the heap surface.

The second snapshot shows the flow in the configuration when the front of the granular material impinges on the retaining wall. The photograph indicates that vivid particle

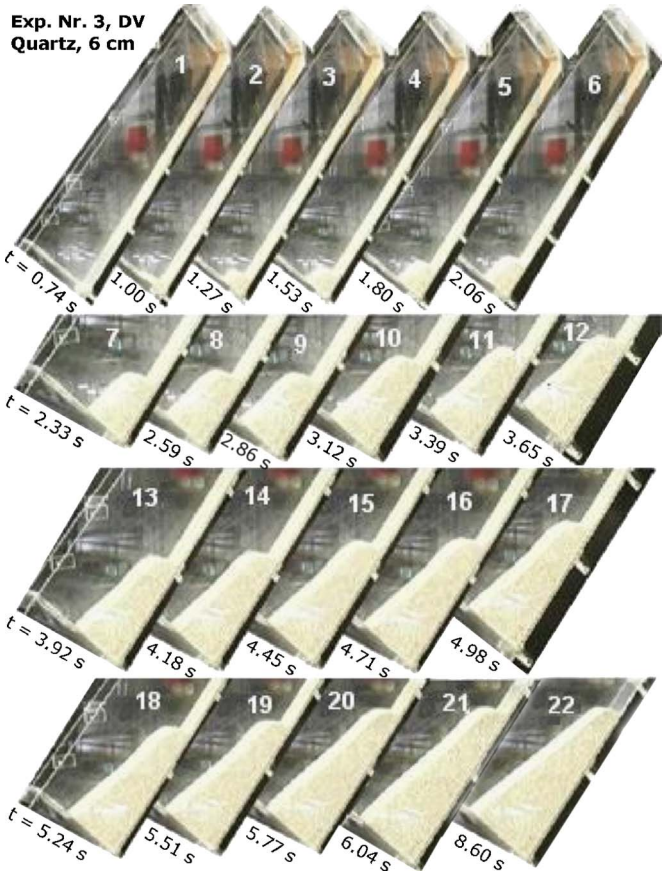

FIG. 3. (Color online) Arrangement of 22 avalanche heaps for Experiment No. 3 arranged in consecutive order taken 0.74–8.60 s after the gate has suddenly been opened with a gap width of 60 mm. The last panel (at $t=8.60$ s) is the final settlement of 15 l of quartz sand. Images were taken by digital video (DV).

bouncing takes place at this instant. The subsequent photographs show how the rapidly moving material between the head gate and the growing deposited pile accumulates mass as long as the granular flux continues from above. Visual inspection of the experiment shows that the rapid flowing material is climbing the deposition heap and quickly comes to rest as the top of the frontal zone is reached. In an analogy to aerodynamics or hydraulics, the transition region from the rapid, supercritical flow to the stagnant heap will be called a

FIG. 4. (Color online) Same as Fig. 3 but for $t \geqslant 8.60$ s, when complete settlement was established.

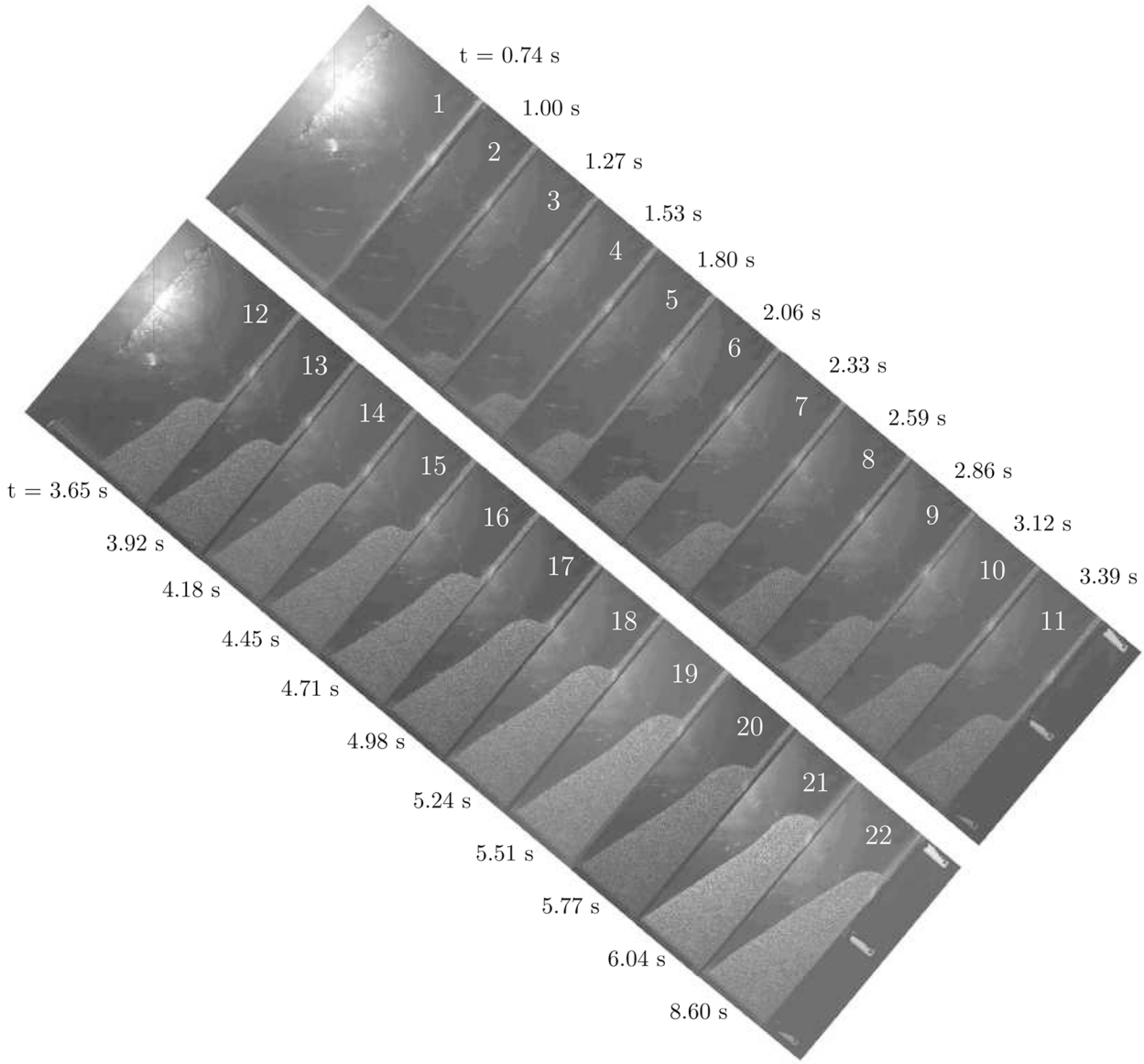

FIG. 5. Snapshots of the flowing granular material (quartz sand) down the inclined chute encountering the retaining wall erected 2 m below the opening gate of the silo. The 22 photographs are taken by the CCD camera at the same times as the video-photographs in Figs. 3 and 4 are recorded.

diffuse shock or a granular jump, "diffuse," because of its considerable width, comparable in size to the heap depth and much larger than a particle diameter.

Comparing the heap forms in the various panels, it is seen that the granular jump first assumes a doubly curved, *S*-shaped form (compare panels 7–19). This shape is preserved as long as the granular flux from above is constant. In the last three panels (panels 20–22) of Fig. 3 the flux is declined and approaching zero in panel 22 (Fig. 4). This is the likely reason why the upper end of the heap is "claw-type" with the steepest angle of inclination of the surface at the *contact line* with the bottom. This shape is maintained for the final heap at rest when all 15 l of quartz grains have moved down, and all motion has ceased (Fig. 4). One additional, curious observation is the fact that the heap takes its largest depth at the retaining wall. This height is decreasing as one moves away from this wall. The decrease is approximately linear with the distance from the wall, except that a slight declination of the surface profile is discernible in the last two or three panels of Figs. 3 and 4. The surface slope apparently adjusts to the angle of repose of the material which in this case is equal to the internal angle of friction $\phi = 33°$, which agrees well with corresponding measurements from the photographs.

Very similar behavior can also be inferred from the photographs of the CCD PIV-CAM camera, reproduced in Fig. 5 and corresponding velocity fields in Figs. 6 and 7. The early *S*-shaped profiles of the granular jumps and their transformation into a claw are also seen here, however, with less conspicuous formation of the small declination of the free surface upon the cessation of the flux from above. It is, moreover, worth noting that the CCD photographs of Fig. 5 and their respective velocity fields of Figs. 6 and 7 equally disclose an angle of repose of the stagnant heap of $\approx 33°$

agreeing with the internal friction angle $\phi=33°$. Velocities were deduced from the CCD images captured by using the PIV-CAM and the PIV system. Velocity vector plots in color are summarized in Figs. 6 and 7.

Since for each panel the velocity magnitude is scaled to its maximum value, we separately list the maximum (and minimum) velocities of the selected 11 panels in Figs. 6 and 7 and in Table II. These are from 0.0 (standstill) to 4.10 m s^{-1} in the supercritical regime of panel 3 in Fig. 6 (note that panel 2 is not shown here and in panel 1 flow is only in the inclined part and does not hit the front wall). It is also clearly evident that only in the early heap formation, there are significant velocities within the heap, and even then, practically only in the granular jump region, and they

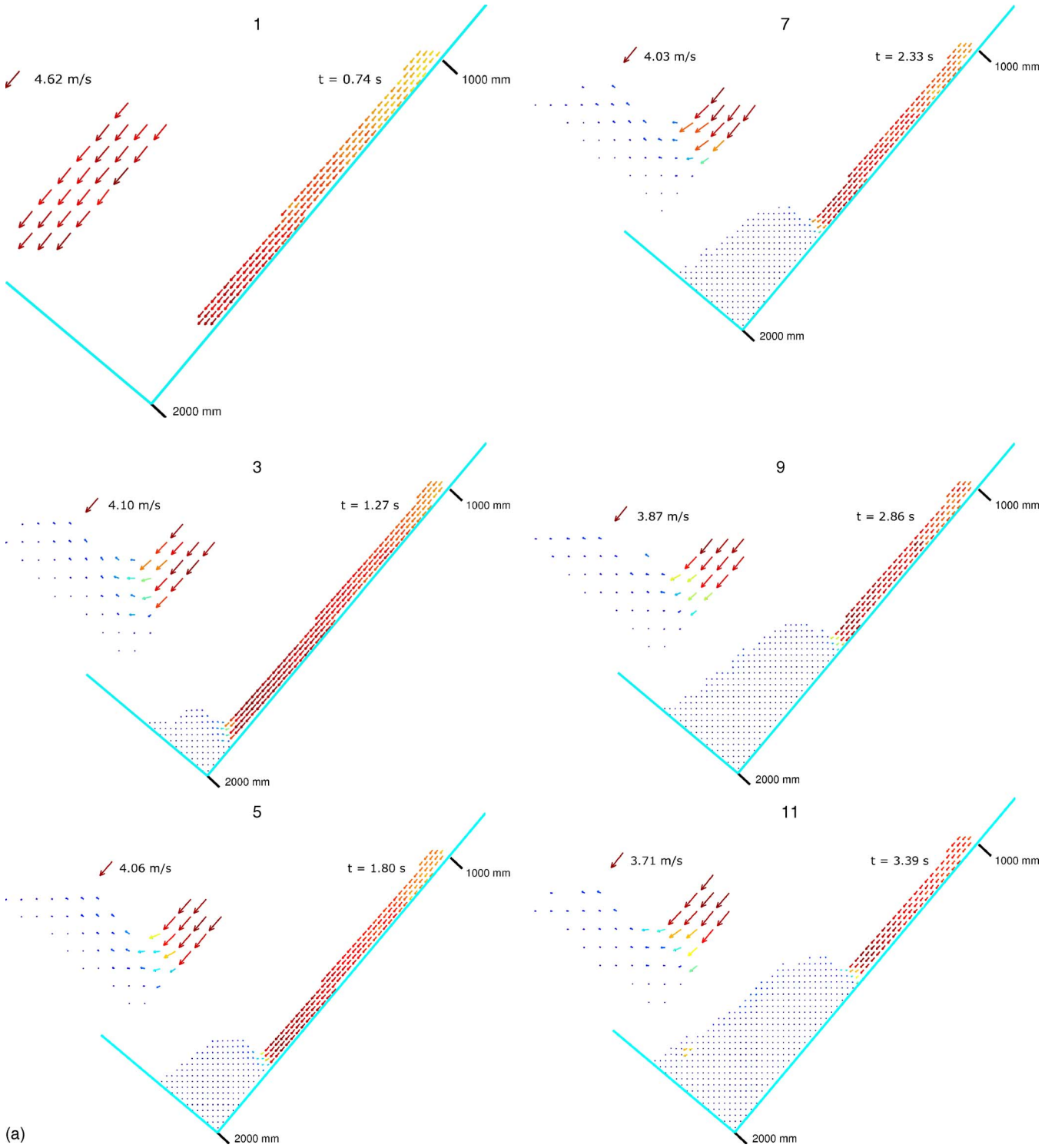

FIG. 6. (Color online) Velocity plots, generated by the PIV software from the CCD photographs. The color code is scaled with the maximum velocities whose values are given in Table II. The numbers correspond to the panel numbers in Figs. 3 and 5. Enlargements of the flows in the vicinity of the shock fronts are shown in the insets in each panel.

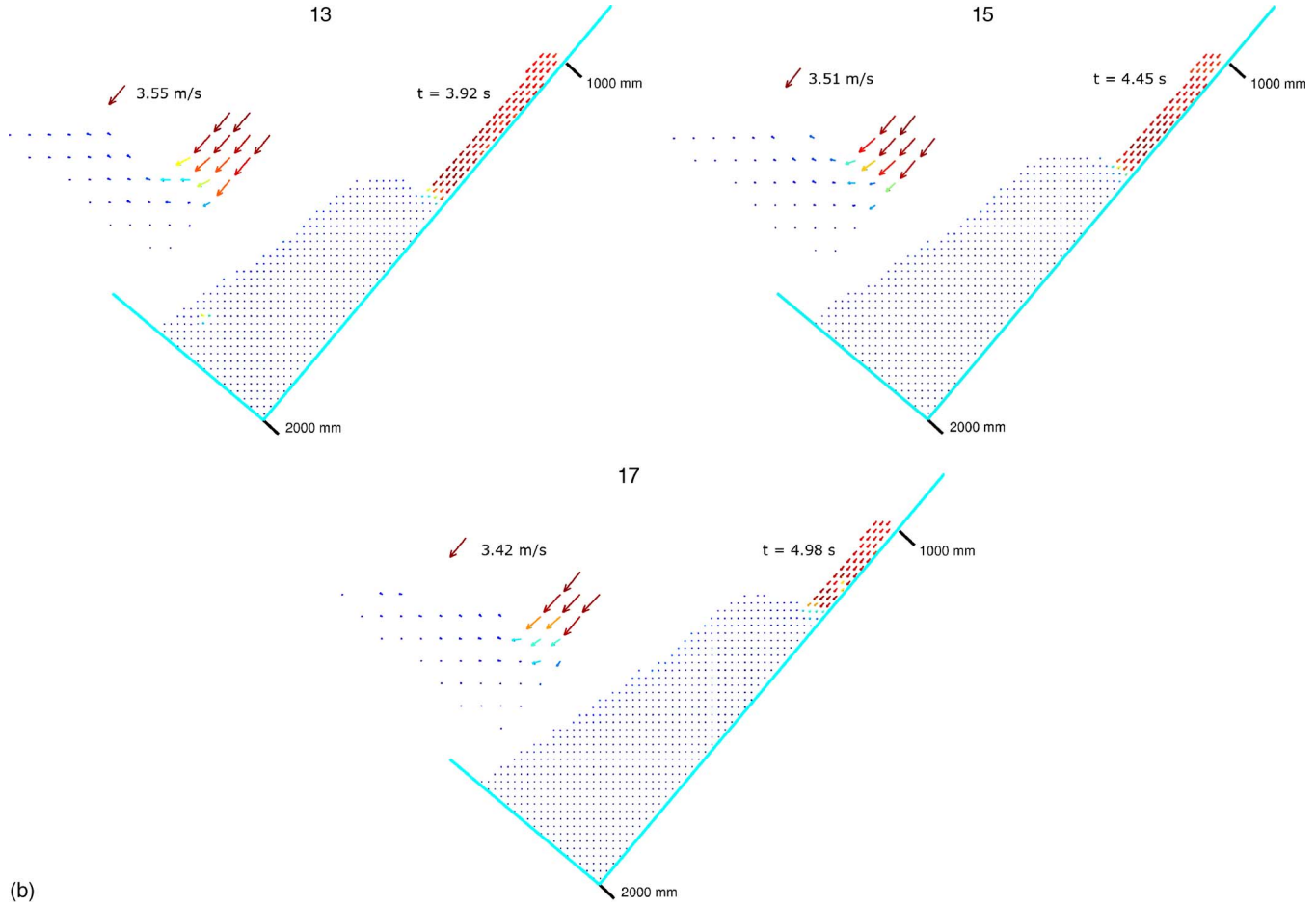

FIG. 6. (*Continued*).

are restricted to a surface near the boundary layer. At later times, e.g., panels 19 and 20, only sporadic nonvanishing very small surface motion takes place within the heap, perhaps interpretable as particle rearrangements on the surface. This latter motion seems to be largely incoherent, intermittent, and of a repetitive nature.

It should be emphasized that the direction of the motion changes drastically, when the particles move from the thin layer into the granular jump regime. There, the flow quickly turns from a bottom-parallel motion to an essentially bottom-perpendicular direction, where the particles seem to come to rest. Only few particles continue to move further and leave the diffuse shock region, rearrange themselves, and (perhaps) smooth the slightly uneven top surface.

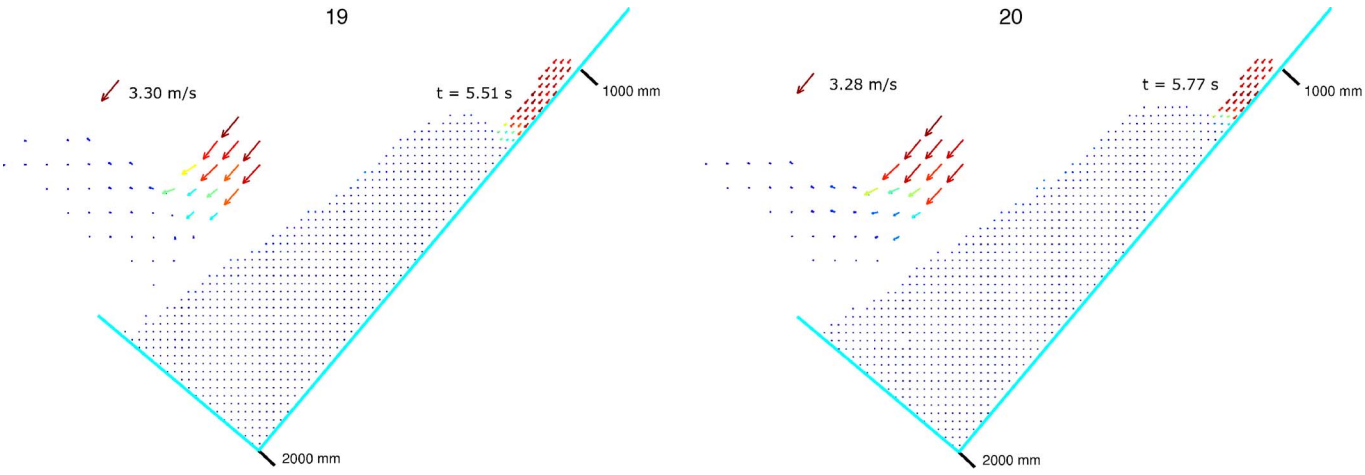

FIG. 7. (Color online) Continuation from Fig. 6. Last panels, close to final deposit.

TABLE II. Maximum and minimum velocities in 11 panels of Figs. 6 and 7. The panel numbers correspond to respective panels in Figs. 3 and 5 (Experiment No. 3).

Panel	Max. vel. ($m\ s^{-1}$)	Min. vel. ($m\ s^{-1}$)	Panel	Max. vel. ($m\ s^{-1}$)	Min. vel. ($m\ s^{-1}$)
1	4.62	3.00	13	3.55	0.00
3	4.10	0.00	15	3.51	0.00
5	4.06	0.00	17	3.42	0.00
7	4.03	0.00	19	3.30	0.00
9	3.87	0.00	20	3.28	0.00
11	3.71	0.00			

B. Experiment No. 5

The evolution of the pile buildup for the motion of the quartz particles through the gate with the 6 cm gap width is shown in Fig. 8. Here, the retaining wall is within the horizontal runout zone, 0.63 m downflow from the abrupt transition point into the horizontal portion of the chute. In the first panel (shot 1 after the onset of the motion at $t=0.80$ s) the flow front just hits the surface of the horizontal plane with very high impact. The second panel shows the thin, rapidly moving layer, immediately after impinging the retaining wall, barely displaying the granular shock; it took approximately 1.33 s after the opening of the head gate, until the front encountered the wall. The third panel shows how the stagnant heap grows backward along the horizontal leg of the chute. The backward moving front in this panel has a smooth transition from supercritical to subcritical motion. The jump in height is relatively small when compared with Fig. 3; interestingly, the thickness of the heap grows with distance from the retaining wall, though only slightly. The subsequent panels 4–12 ($t=2.39-6.63$ s) show how the heap "climbs" up the inclined portion of the chute according to the granular flux that is provided from above until it comes to rest at $t>6.63$ s. The free surface in this steep portion of the deposit is steeper than that in the horizontal distal part, but when compared with the deposits analogous to those in Fig. 3 the free surface inclinations of the steep portions are—to within experimental error—analogous, namely ~33°, equal to the angle of repose of the heap (which, as before, is roughly equal to the internal angle of friction). So the granular material arranges itself to form a wedge-type deposit.

FIG. 8. (Color online) Arrangement of 12 avalanche heaps in Experiment No. 5 arranged in consecutive order, taken 0.80–6.63 s after the gate opening of the 6 cm gap width. The granular flux down the inclined chute terminates between $t=6.10$ s and $t=6.63$ s.

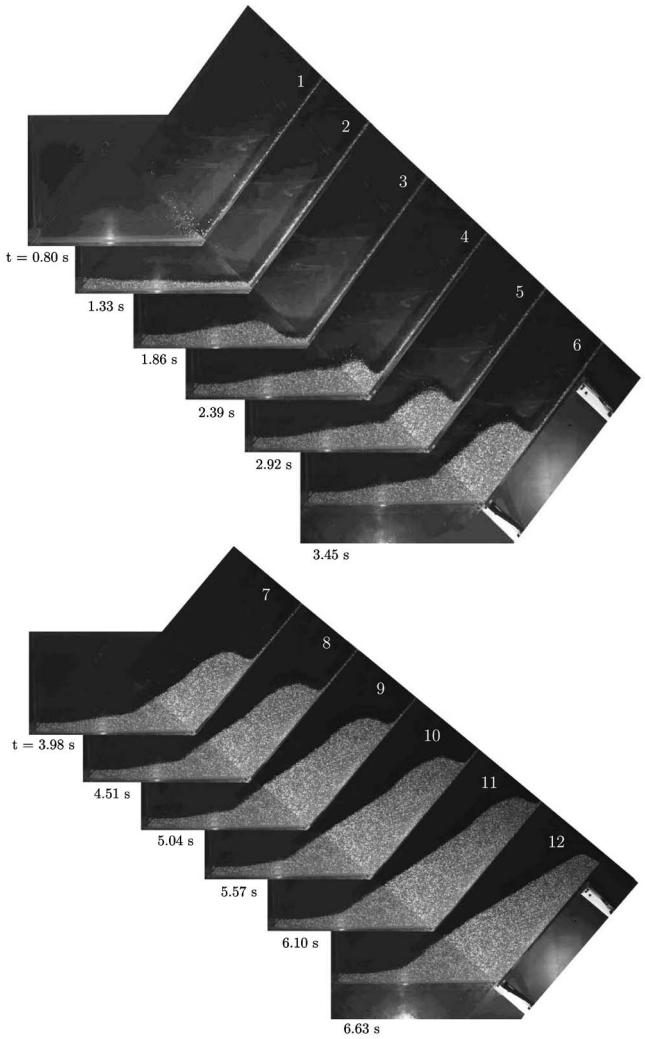

FIG. 9. Arrangement of 12 avalanche heaps in Experiment No. 5 arranged in consecutive order, taken 0.80–6.63 s after the gate opening of the 6 cm gap width. The granular flux down the inclined chute terminates between $t=6.10$ s and $t=6.63$ s.

Figure 9 shows 12 snapshots of the CCD images and Figs. 10 and 11 display the velocity plots as inferred via the PIV system. As expected, the velocities are large—supercritical—in the inclined portion of the chute before the *granular jump*. The transition from the thin layer via the *diffuse jump* into the stagnant heap is again achieved with a substantial change of the modulus and direction of the velocities at the backward (upslope) moving front of the heap. This transition is, however, different for jumps in the horizontal and inclined parts of the chute. From the first two panels of Fig. 10 it appears as if a first jump arises at the kink of the inclined to the horizontal part, while a second much more diffuse transition also occurs as a result of the abrupt secession of the motion due to the retaining wall. When the stagnant heap reaches the inclined part of the chute, only a

single shock occurs. Its form is *S*-shaped. A free surface occurs with only one single sign of the curvature with a tangent at the "contact-line" that is perpendicular to the bed. These features are corroborated by the CCD images in Fig. 9.

Table III lists the maximum and minimum velocities that were determined in each panel of Fig. 10. They range from zero values to a maximum of 4.95 m s^{-1} in panel 1. However, with respect to the upward moving shock in the inclined part of the chute the maximum velocity takes place in the fourth panel which is 4.42 m s^{-1}. The result is interesting that in panel 11, in which the material is at rest, speeds arise which are as large as 3.4 m s^{-1}. Scrutiny shows that they occur only sporadically and may be attributed to individual particles that fall into holes immediately below them. Afterwards, the material body was completely at rest, panel 12 in Fig. 9.

V. ANALYSIS OF THE DATA

The major event of interest to us here is the transformation of the flow from the inclined part to the horizontal part of the channel. As a consequence of that the material is encountering the retaining wall at the base of the inclined chute or in the horizontal runout zone. In the early stage of this transitional motion, the granular material climbs up the wall with violent bouncing, but the motion is quickly reduced and then stopped by the flux of material approaching from behind. A heap of considerable height is formed, which grows in length as particles accumulate from behind, as long as the particle flow continues from the head gate at the upper end of the inclined chute. The approaching particles climb the steep rear end of the heap with considerable speed and come to rest soon after having reached its upper flank. Meanwhile the

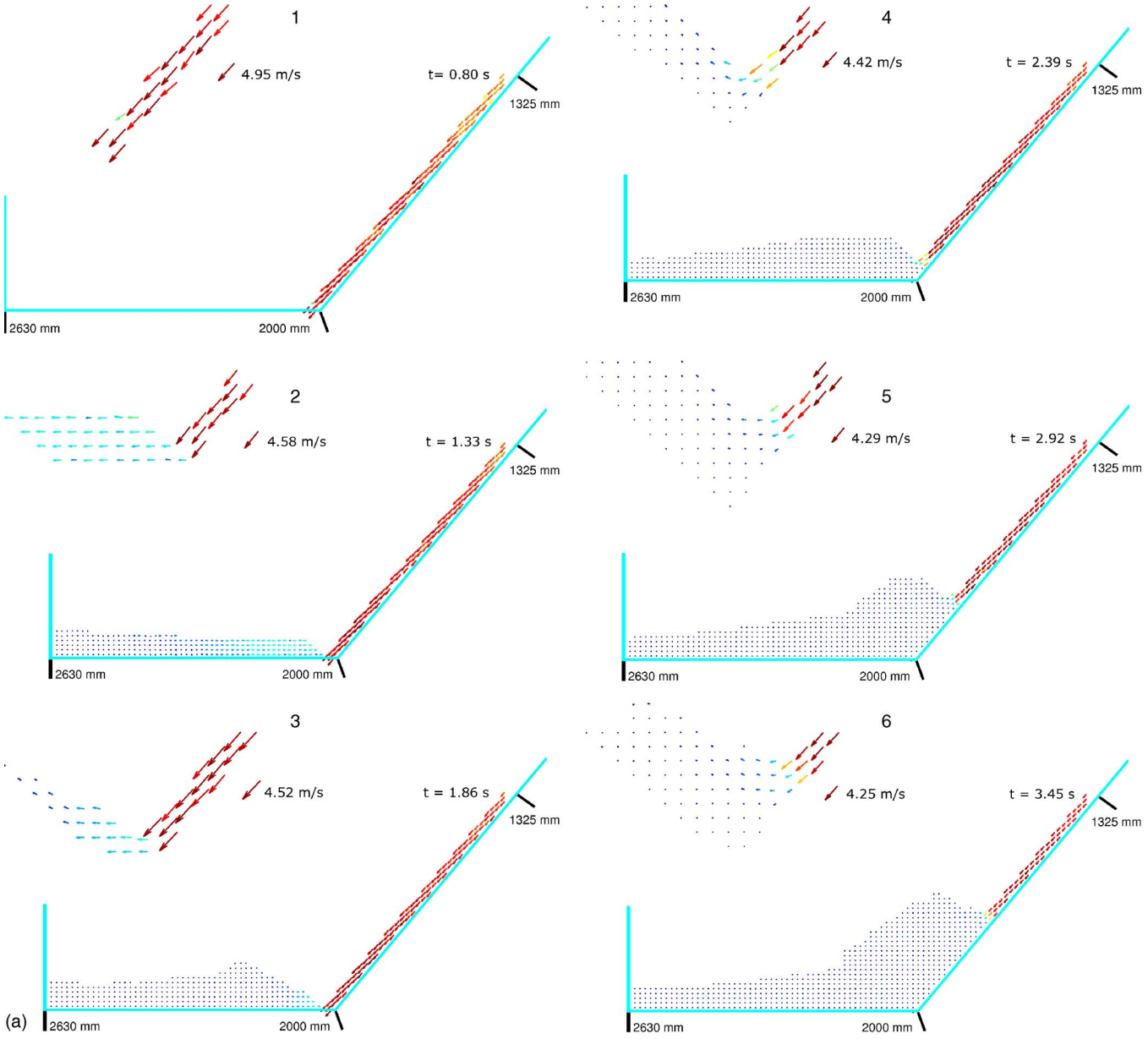

FIG. 10. (Color online) Velocity plots, generated by the PIV software from the CCD images in Fig. 9. The velocity profiles are scaled with the maximum values of the velocity magnitude as given in Table III. Enlargements of the flows in the vicinity of the shock fronts are shown in the insets in each panel.

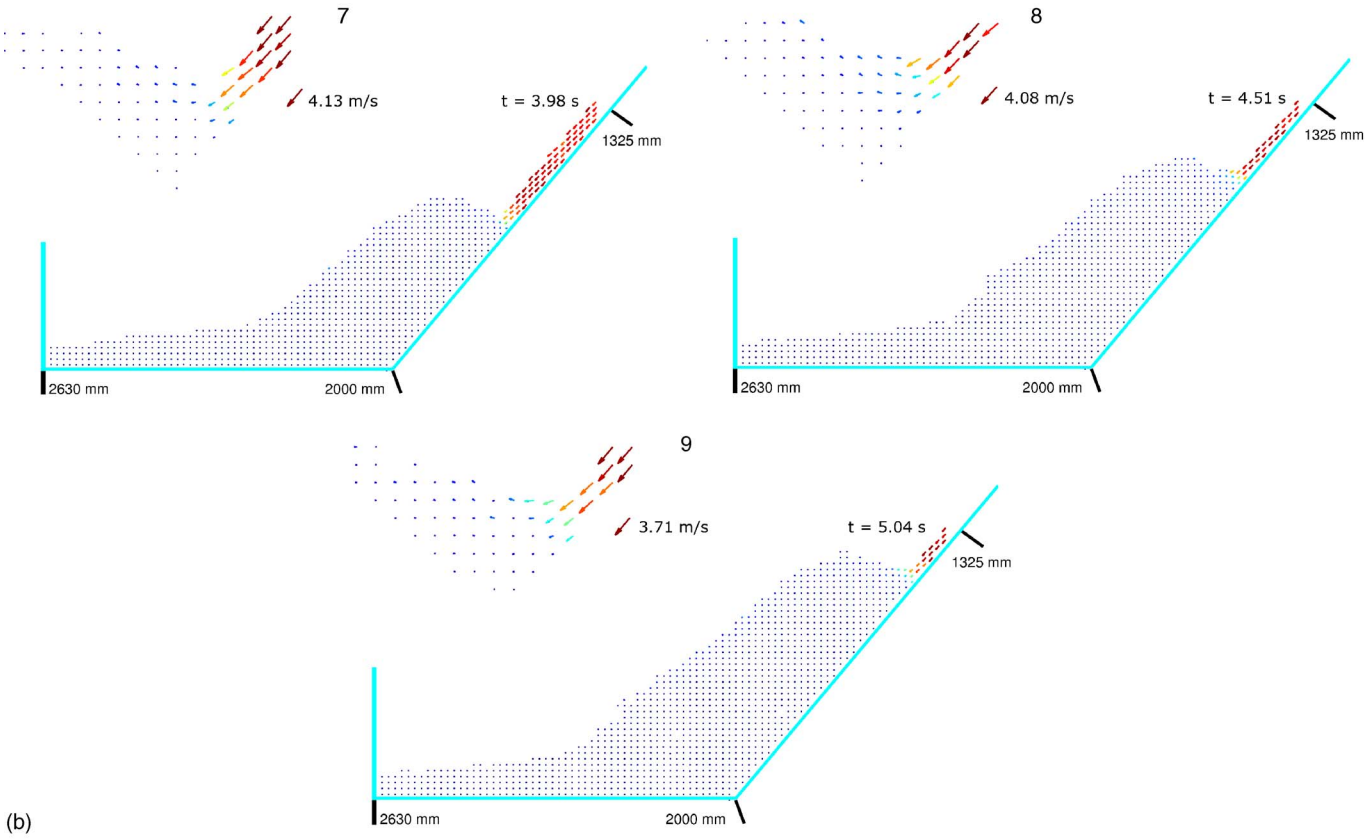

FIG. 10. (*Continued*).

rear end accumulates mass and moves backwards with a speed of propagation, which itself is determined by the height of the heap at its rear end and the flux of mass from above. With reference to Fig. 12, which approximates the smooth transition as a jump discontinuity, a simple mass balance yields

$$c(H-h) = vh = Q \tag{1}$$

or

$$c = \frac{Q}{H - \frac{Q}{v}} = \frac{Q}{H-h}, \tag{2}$$

in which Q is the volume flux from above, H and h are the flow depths in the heap and before it, v is the approaching supercritical velocity in the approaching flow, and c is the backward moving velocity of the shock.

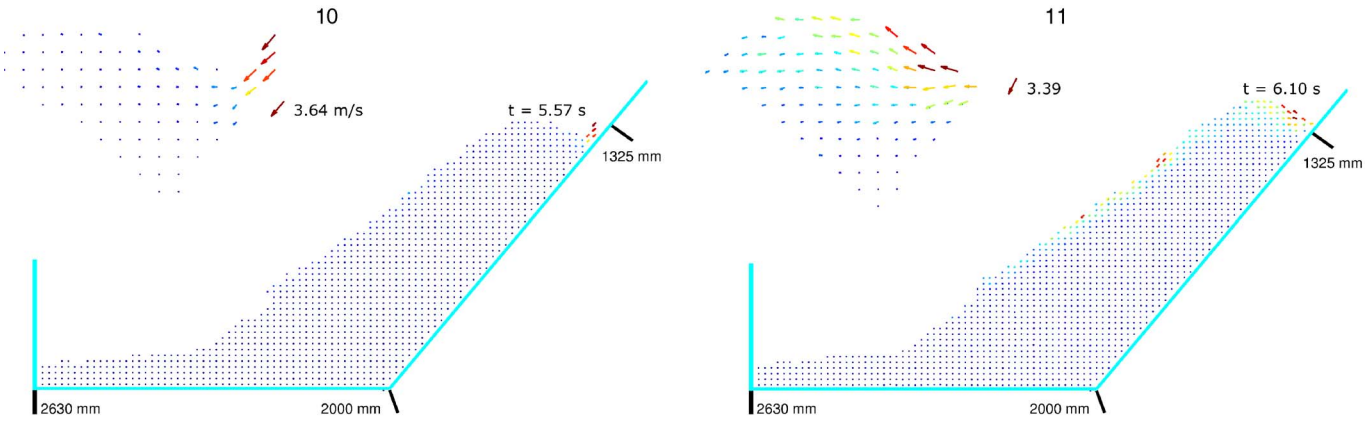

FIG. 11. (Color online) Continuation from Fig. 10, panels close to deposition.

TABLE III. Maximum and minimum velocities in panels 1–12 of Figs. 10 and 11 (Experiment No. 5).

Panel	Max. vel. ($m\ s^{-1}$)	Min. vel. ($m\ s^{-1}$)	Panel	Max. vel. ($m\ s^{-1}$)	Min. vel. ($m\ s^{-1}$)
1	4.95	0.18	7	4.13	0.00
2	4.58	0.00	8	4.08	0.00
3	4.52	0.00	9	3.71	0.00
4	4.42	0.00	10	3.64	0.00
5	4.29	0.00	11	3.39	0.00
6	4.25	0.00	12	0.00	0.00

In this section we will analyze the maximum velocity, impact velocity, flow height, impact velocity versus flow height, channel length against impact momentum, hydraulic jump or shock velocity, total height of the shock front from the measurements and the same as predicted from a semianalytical method by using simple mass balance. For the prediction of the above mentioned variables, the mass balance equation (1) or (2) and Fig. 12 will be implemented, while the experimental data are taken from Figs. 5–7 (Experiment No. 3).

A. Maximum velocity and impact velocity of the flow

The PIV measurement technique is very useful to determine the velocity distribution, particularly the impact velocity in granular flows hitting an obstruction. The maximum velocity arises either at the instance when the flow hits the wall or in the subsequent images just in front of the shock front. In Fig. 13 the maximum velocity versus the flow length is plotted. The largest velocity, 4.1 $m\ s^{-1}$, is seen at the instant after the flowing granular mass hits the front wall erected normal to the basal surface (panel 3 in Figs. 3, 5, and 6). The maximum velocity first decreases gently then more rapidly and finally the decrease is less rapid again. It indicates development and disappearance of small surges in the granular flows in the narrow rectangular channel. The likely source of the surges may be limited jamming in the silo gate which might have produced intermittent flows. Other sources might be generation and settlement of shock fronts because sometimes the fronts are more agitated while in other cases they are less. Finally, the maximum velocity drops to 3.28 $m\ s^{-1}$; compare with the 20th frame in Figs. 3, 5, and 6. So, the maximum velocity decreases almost linearly, but with some disturbances, as the shock front travels upslope.

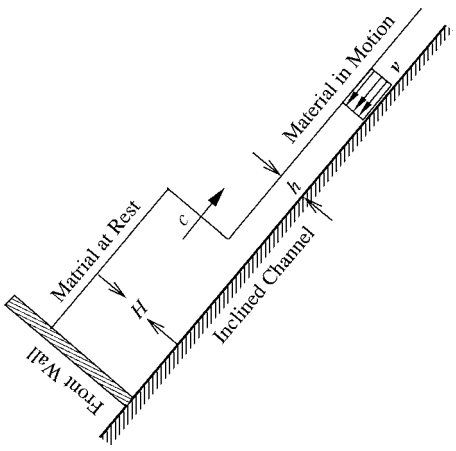

FIG. 12. Flow of granular material with speed v and height h, approaching a heap of height H at rest. Mass balance then requires $c=Q/(H-h)$ as speed of the growth of the heap at rest, where Q is the volume flux of mass from above.

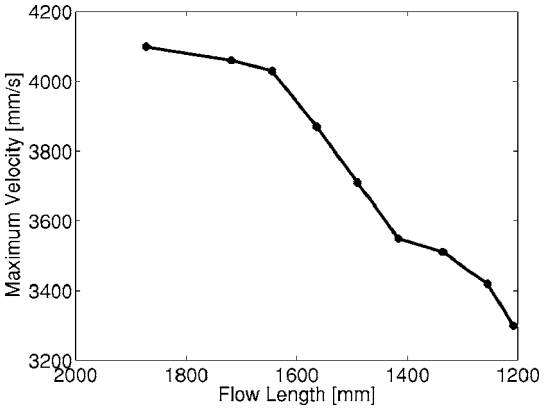

FIG. 13. Evolution of the maximum velocity of the flow in front of the shock. The maximum velocity is decreasing almost linearly as the shock front induced by the dry granular flow travels upslope from the vicinity of the front wall in the lower end of the narrow rectangular channel. Dots, from upper left to lower right, represent values as obtained from the PIV measurements in panels 3, 5, 7, 9, 11, 13, 15, 17, and 19, respectively, in Figs. 6 and 7. "Flow Length" = distance from gate to shock position.

We define the impact velocity to be the velocity immediately before the hydraulic jump where the flow height is minimal. This is clearly identifiable in Figs. 5 and 6 as the "terminal" velocity in front of the hydraulic jump as indicated by the multicolored sheared layer. It is very interesting to note that the impact velocity, following the maximum velocity, is much smaller than the maximum velocity. Although the maximum velocity occurs only some millimeter distance upstream of the channel from the shock front, the drop from the maximum velocity to the impact velocity is rapid. This is due to the very fast decelerating motion. It is found that the decrease from the maximum to the impact velocity is almost linear and amounts to 39% downstream and 25% upstream of the maximum velocity. This means, it varies from 1.6–0.82 $m\ s^{-1}$. The evolution of the impact velocity is depicted in Fig. 14.

Information on the impact velocity is very important from a structural engineering point of view. In mountainous regions prone to avalanche or debris flows, civil engineers must know the impact pressures that can be induced by possible natural events. The wall of a house or any other infrastructure facing the slope of a mountain must be able to withstand the impact pressure associated with such natural events so as to reduce any casualties.

B. Flow height

It is very difficult to experimentally determine the actual flow depth of the flowing granular material in the inclined long channel because the flow is sheared immediately below

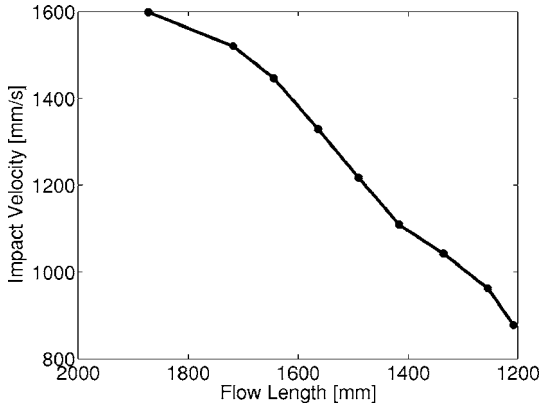

FIG. 14. Impact velocity versus flow length: Impact velocity is decreasing almost linearly as the shock front induced by the dry granular flow travels upslope from the vicinity of the front wall in the lower end of the narrow rectangular channel. Dots, from upper left to lower right, represent values as obtained from the PIV measurements in panels 3, 5, 7, 9, 11, 13, 15, 17, and 19, respectively, in Figs. 6 and 7. "Flow Length" = distance from gate to shock position.

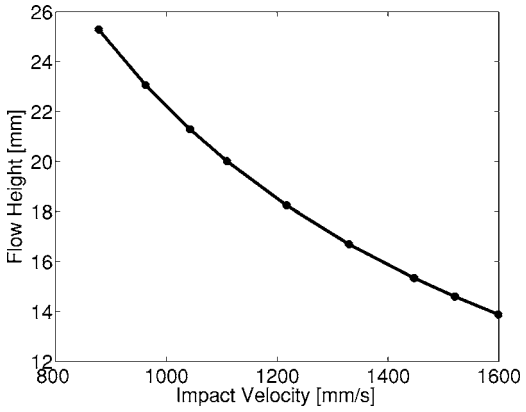

FIG. 16. Flow height versus impact velocity: Dots, from upper left to lower right, represent values as obtained from the PIV measurements in panels 3, 5, 7, 9, 11, 13, 15, 17, and 19, respectively, in Figs. 6 and 7.

the silo gate so that its depth averaged velocity is difficult to determine, and it is quickly thinning as the flow is accelerated as the head travels down the incline. Since the opening of the head gate in our case is only 6 cm and the travel distance in the inclined chute is 2 m the flow depth at the lower end of the channel will be only some particle diameters or a few mm. However, accurate knowledge is very important for the study of the dynamic behavior of the flow.

Equations (1) or (2) can be used to estimate the flow depth of the granular mass in the channel. We know from the PIV measurement the inflow velocity of the granular particles leaving the silo to be close to 0.37 m s^{-1}. The silo height is 0.06 m. The mass flux is $Q=0.0222$ m^2 s^{-1}. On the other hand, we have the following relationship from conservation of mass:

$$Q = Q_i = h_s v_s = h_i v_i, \quad \text{or} \quad h_i = Q/v_i, \tag{3}$$

where the indices s and i stand for the variables at the silo gate and at the position of impact, respectively. Since we know Q and the impact velocity, we can estimate the flow height in the vicinity of the shock front by using relation (3). Results thus obtained are plotted in Fig. 15. It shows that the flow height increases, first slowly, then faster, from about 14 mm at the lower end of the channel to 26 mm close to the final deposit of the mass just upslope of the heap, about 1200 mm from the silo gate. Since the mean particle diameter is about 4 mm, the depth of the flow varies from about 3.5 particle diameters in the vicinity of the front wall to about 6.5 particle diameters about 800 mm upslope from the impact wall. Note that the flow height at the silo gate was 15 particle diameters. This means that the variation of the flow height at the far end of the channel varies slowly.

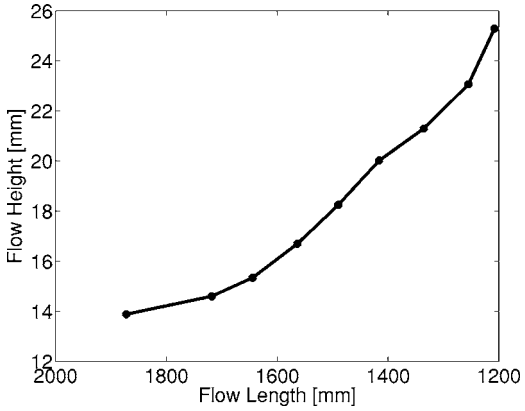

FIG. 15. Flow height versus flow length: Flow height is increasing as the granular shock front moves upslope from the front wall in the lower end of the narrow rectangular channel. Dots, from lower left to upper right, represent values as obtained from the PIV measurements in panels 3, 5, 7, 9, 11, 13, 15, 17, and 19, respectively, in Figs. 6 and 7. "Flow Length" = distance from gate to shock position.

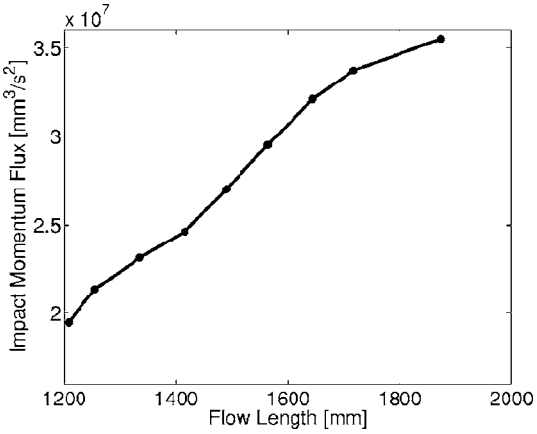

FIG. 17. Impact momentum flux versus flow length: Impact momentum flux is decreasing as the granular shock front moves upslope from the retaining wall to the final position of the tip deposit. Dots, from lower left to upper right, represent values as obtained from the PIV measurements in panels 3, 5, 7, 9, 11, 13, 15, 17, and 19, respectively, in Figs. 6 and 7. "Flow Length" = distance from gate to shock position.

C. Impact velocity versus flow height

It is also important to know the relationship between the flow height and impact velocity because this information is needed to determine the stagnation pressure. The height at the transition point to the deposit versus the impact velocity is shown in Fig. 16. The height at the transition point is indicated by the foot of the line T1 in Fig. 19, which, as discussed in Sec. V A, is the point just in front of the hydraulic jump. Since the hydraulic jump is a bit "diffuse," it is better to call it a small "transition region" in which the impact velocity turned out to be a strict function of position of the transition region in the chute since the flow accelerates from rest until impact. As the impact velocity decreases, the flow height increases with the growth of the deposited mass. The deviation of the curve from linearity is manifestation of the nonsteadiness of the flow in the upslope regime.

D. Impact momentum flux

Dynamically the impact momentum flux, hv^2 is perhaps the most important quantity. Since the impact momentum flux is proportional to the square of the impact velocity, it is dramatically decreasing as the deposit moves into the upslope regime, showing a dominant effect of the impact velocity against flow height. This is shown in Fig. 17.

E. Shock velocity

The shock velocity is an interesting and important quantity for the description of the shock propagation because it provides us with a connection between flow height, impact velocity and the height and velocity of the moving shock front. The shock speed could either be estimated from the mass balance (1) or (2) which provide a relation for the flow height, height of the shock front and impact velocity. Since the shock front is diffusive, it is not directly possible to predict the shock speed from the mass balance equation. However, we can easily and explicitly compute the shock speed from the photographs taken from the high resolution CCD images because we know the positions and the displacements of the shock front at the recorded times. As obtained from the CCD images, the shock velocity is fluctuating in a certain band width as shown in Fig. 18 with the maximum and minimum values between 168 mm s^{-1} and 149 mm s^{-1}, respectively, and the mean value at 160 mm s^{-1} (with an uncertainty of about 6%). As already discussed, the reason might be the development of intermittent flow, small surges induced by the granular jamming in the silo gate, instabilities in the region of the shock front and highly bouncing particles, which are first agitated as they hit the shock front and then settle down in a short span of time.

F. Estimated height of the shock front

Since $H=Q/c+h$, it is now possible to estimate the height of the shock front in the vicinity of the impact position from the information derived above: Q is derived from the initial condition, geometry of the opening of the silo gate and the conservation of mass; c is measured from the CCD images; h is derived from conservation of mass and the PIV data of impact velocity. In this way, H can be determined semianalytically. The height of the shock front thus obtained is plotted in blue in Fig. 20. Since it involves the conservation of mass, a relationship among the variables in the vicinity of the shock front, and the measured data, we will call this result a predicted result. Figure 20 (blue line) shows that the height of the shock front is fluctuating in a certain band width just as the shock velocity does, because both variables are (almost) inversely proportional to each other. Note that, since h is very small compared to H, the influence of h could be neglected. However, in our calculation we will include it; its mean contribution to the height of the shock front is about 12.5%.

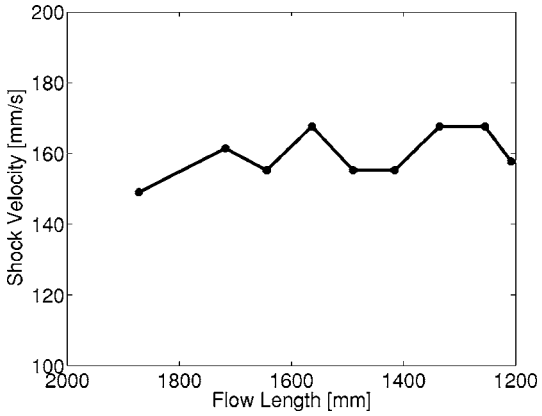

FIG. 18. Shock velocity versus flow length: Shock velocity is fluctuating in a certain band width with maximum and minimum values between 168 mm s^{-1} and 149 mm s^{-1}, respectively; the mean value is 160 mm s^{-1}. Dots, from left to right, represent values as obtained from the PIV measurements in panels 3, 5, 7, 9, 11, 13, 15, 17, and 19, respectively, in Figs. 6 and 7. "Flow Length" = distance from gate to shock position.

G. Prediction of the height of the shock front

As explained above, we now have a systematic estimation of the evolution of the shock front from the measured impact velocity, the mass balance equation, and the dynamic flow height. These informations were sufficient to let us evaluate the shock-front height semianalytically in the granular flow. Now we are in the position to check whether we could directly obtain the evolution of the height of the shock front and if there is any correlation with the information depicted in Fig. 20 (in blue) as obtained by using the semiexact method. For this reason we analyze the CCD images as shown in Fig. 5. Since the shock front is not sharp but diffuse, we could not easily determine the height of the shock from direct measurement. Therefore, we need a "definition" of the shock front. This is explained in Fig. 19 and its caption. The shock behavior in the granular flow can be divided into two parts: "rise" (T1, tangent at the front slope) and "settlement" (T2, tangent at the rear slope). In T1 the flow is rising, and in T2 the mass is settling down, capturing the entire dynamics of the shock front. Therefore, T1 and T2 together represent the transition of the flow from the supercritical to the subcritical state. For this reason we take the interception of the tangents connecting the front (T1) and rear (T2) slopes of the body as shown in Fig. 19; then the

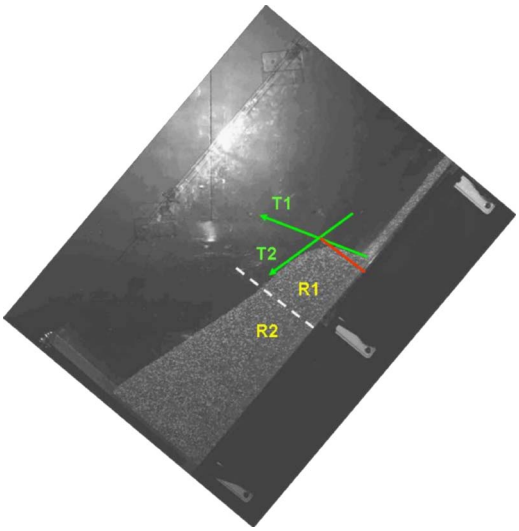

FIG. 19. (Color online) Graphical interpretation of the shock height: The shock behavior in a granular flow can be divided into two parts: "rise" (T1) and "settlement" (T2). Taking the interception of the tangents connecting the front (T1) and rear (T2) slopes of the body, the shock front height is taken to be the distance of this point from the sliding base of the channel (red line). The white dashed line passes through the point of concavity. This line divides the (almost) deposited body into two parts: on the surface of region R1 the particles are in bouncing motion, while at the surface of R2 they are in contact with the main dense body. This image is the 20th panel in Figs. 5 and 21.

shock-front height is taken to be the distance of this point from the sliding base of the channel (red line). The shock heights thus determined are plotted in Fig. 20 in red. Since this involves only measurement data, the height thus obtained is called experimental (measurement).

Comparison of some representative and basic data would help to understand the validity of the procedure which we have used in the determination of the shock-front height. The computed maximum, minimum, mean, and standard deviation of the shock front height are 166 mm, 149 mm, 158 mm, and 0.0057 mm (with an uncertainty of about 6%), respectively, while these values for the direct measurements are 164 mm, 151 mm, 158 mm, and 0.0052. The correlation coefficient is 0.89. This shows that there is a close relationship between measurement and estimated shock height evolution as depicted in Fig. 20. Therefore, both ways of determining the shock-front heights seem to be useful in practical applications.

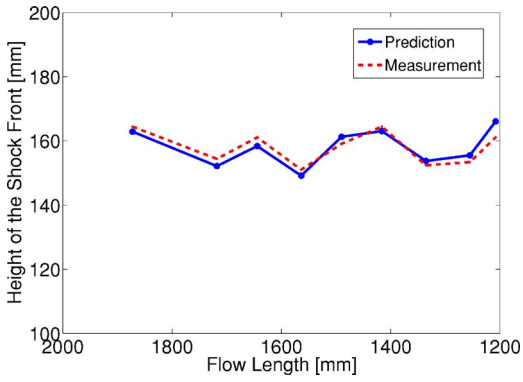

FIG. 20. (Color online) Evolution of the height of the shock front as determined by the measurements and the semianalytical method. Dots, from left to right, represent values as obtained from the PIV measurements in panels 3, 5, 7, 9, 11, 13, 15, 17, and 19, respectively, in Figs. 6 and 7. "Flow Length" = distance from gate to shock position.

VI. EVOLUTION OF THE SURFACE GEOMETRY

As seen in Fig. 21, the evolution of the surface geometry of the near deposit granular body passes from concave to convex structures and finally settles as a straight inclined surface. In Fig. 19 the white straight line perpendicular to the sliding bed passes through the point of concavity. This line divides the (almost) deposited body into two parts: on the surface of region R1 the particles are in ballistic motion, but on the surface of R2 they are in contact with the main dense body. In Fig. 21, the white straight lines form the envelopes of the deposition near the wall and touch the maximum point of the diffusive shock front. The first panel is the 20th image of Experiment No. 3 which shows that the flow from upstream is still continuing, while the second panel is the 21st image in which the flow from above has just (almost) ceased. In the third panel settlement behavior is seen both in the front and on the surface of the body, but afterwards from panels 4–7 little motion and rearrangement of the particles occurs only on the free surface and in a very thin layer below the free surface. In the first two panels, the white lines constitute the straight envelopes to the free surface of the body; vacua between these white lines and the concave surfaces of the granular masses can be seen. In the third panel, the mass from the top free surface of region R1 migrates to region R2 thus filling the "concave gap" seen in the previous two panels. The free-surface is then convex. The peak of the convex surface continuously migrates downslope, thus preserving the convexity. Finally, in the last two panels the white lines exactly fit the free surface of the completely settled granular deposit in the inclined rectangular channel. The slope of this free surface is the critical angle of repose of the granular material, which, in turn, is very close to the internal angle of friction of the granular material, $\phi = 33°$.

VII. MEASUREMENT ERROR

Here, we will discuss two types of errors: (I) related to the initial and boundary conditions, and (II) related to the measurement devices, experimental setup, and the material in use.

(I) Error related to the initial and boundary conditions: Since the quartz particles used in the experiments are relatively big (mean diameter of 4 mm), no considerable electrostatic charging was induced during the granular flow by the Plexiglas channel. However, to eliminate the effect of nominal electrostatic charging antielectrostatic spray was used after each experiment. The main reason for using such spray is that it maintains the bed friction angle at constant level. After running the experiments it is observed that the channel is covered by dust due to abrasion during motion. The powdery grains produced by the abrasion can reduce the bed friction angle considerably. It is observed in the laboratory runs and in the numerical simulations that a relatively small change in the bed friction angle influences in the dynamics of the flow,

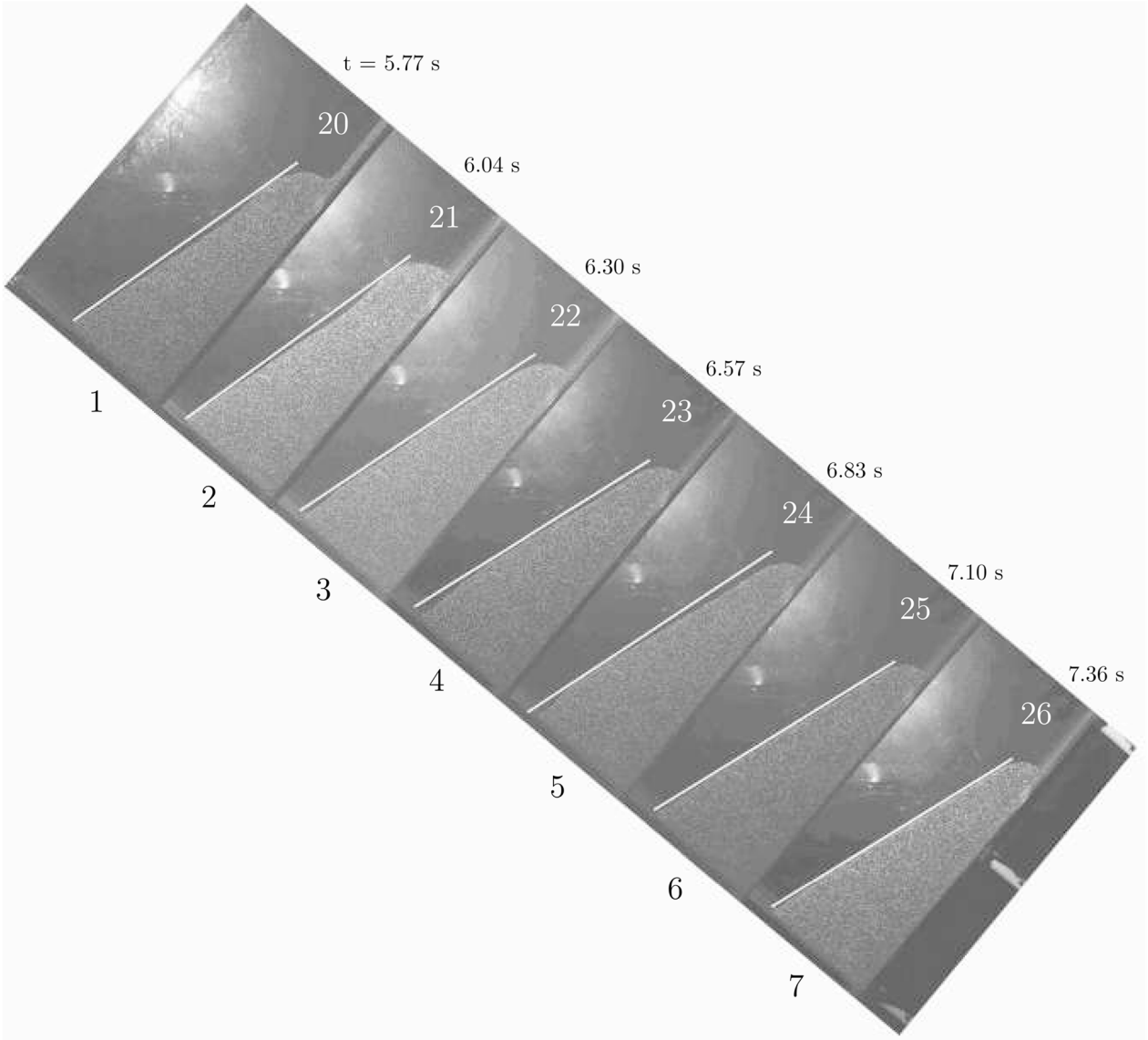

FIG. 21. Evolution of the surface geometry: from concave to convex and then straight with inclination equal to the angle of repose of the granular material, ϕ=33°. In the first panel upstream flow prevails, in the second panel this flow has (almost) ceased. The last two panels show that the granular body has come to a complete standstill. Transition from a concave to convex surface took place between the second and the third panels. Panels 3–5 show the downslope migration of the convex surface and the process of the final settlement and arrangement of the particles at the free-surface and in the immediate boundary layer beneath it. Panels 1–7 correspond to the 20th to 26th images in Experiment No. 3 with quartz particles.

mainly due to the reduction of the frictional resistance (energy dissipation) in the bed, the motion becomes more rapid and the travel distance longer. Similarly, the initial condition of the experiments were kept fixed by using exactly the same amount of material of the same grain size distribution. The silo and the head gate were both stable. This indicates that there was almost no error associated with the initial and boundary conditions.

(II) Error related to the measurement devices, setup, material in use and the environment: This type of error is of greater importance. The PIV system we used to produce the data is from the TSI company. The detailed error analysis for general settings of the PIV system and the granular PIV system were discussed in Pudasaini,[4] Pudasaini and Hutter,[6] Pudasaini *et al.*,[9] and Eckart *et al.*[16] However, here we are going to present measurement errors particularly associated with the present measurement.[18]

(A) Error related to the onset of the motion: The CCD cameras used for acquiring the images have limited time resolution: maximum four double frames per second for a single camera, and maximum two double frames per second for double cameras. Since the flow is quite rapid, taking place in a step channel of 50° inclination with the horizontal, it was not possible to detect the exact onset of the motion from the silo gate with the CCD camera. For this we took video recordings (DV) of each experiment, with a time resolution of 25 frames per second. With this high time resolution it was possible to (almost) exactly determine the release time of the mass through the head gate. This reference time was then used for the determination of the absolute time

points of all PIV and DV data plotted in all figures. Therefore, this reference time may also be responsible for adding the time error with a maximum value of $0.04/2\ \mathrm{s}=0.02\ \mathrm{s}$. However, this absolute time error does not influence the accuracy of the velocity data obtained by the PIV-CCD cameras. The velocity fields plotted in this paper are independently and internally computed online by the PIV system, employing the cross-correlation algorithm. This 0.02 s is the absolute shift of the time frames and should be considered while comparing the data of this paper with any numerical computations of the theoretical models under consideration.

(B) Error due to illumination: The error in velocity due to extremely bad illumination is observed to be below $0.07\ \mathrm{m\,s^{-1}}$. It was intentionally produced choosing completely inappropriate positions of the flash lights (use of flash lights is necessary for our system). However, by placing flashes in the proper positions we could almost eliminate this type of error.

(C) Error due to optical surface properties of sand and sand in motion: Quartz sand has an optically structured surface. Our system could measure the velocity of the static "sand-plate" accurately. Therefore, there is no such error.

We performed experiments with a setup of two cameras, an inclined Plexiglas chute and a "rigid avalanching sand-plate." One camera was placed below the chute, capturing the images from below, the other one above it. The measured mean velocity values (without any filters) at the top and bottom were $1.87178\ \mathrm{m\,s^{-1}}$ and $1.86927\ \mathrm{m\,s^{-1}}$, respectively. The deviation between the mean surface and the mean bottom velocities was only 0.13%. However, the deviation between the smallest and the largest velocity values from both sides was approximately 3.5%.

This shows that the surface properties and illumination are the main source of error, whereas the influence of the Plexiglas is negligible. We could detect the velocity down to almost zero magnitude through the Plexiglas.

(D) Error due to the measurement system: The spot size of the interrogation window chosen is sufficiently small, 32×32 pixels in a 1280×1024 pixel resolution of the CCD camera with color depth of 2^{12} bits. This means that $40\times32=1280$ vectors were calculated for the interrogation spot size of 32×32 pixels. The time delay between the two frames is in the order of $1\ \mu\mathrm{s}$.

Deformation within the interrogation spot is neglected. Since images were taken exactly at the boundary of the dense granular flow in the rectangular chute, this is of limited concern for the present analysis. The reason is as follows: The maximum physical length of the captured image is 1000 mm. So, the largest possible error in length in one interrogation spot is $(1000/40)\ \mathrm{mm}=0.025\ \mathrm{m}$, if everything went wrong within some interrogation spot. Its mean value is 0.0125 m. Next, the time difference between the two frames is $1\ \mu\mathrm{s}=1/1000000$ s. Therefore, the measurement device error is $0.0125/1000000\ \mathrm{m\,s^{-1}}$, which is negligible.

Therefore, the total error which we could detect in our measurement is about 3.63% (=3.5% +0.13%). The absolute time shift of about 0.02 s should also be considered while comparing the data with any simulation but this does not influence the quality and reliability of the data and the results presented in this paper.

VIII. CONCLUSION

In this paper we reported on granular chute experiments from a supercritical to a subcritical state into a deposition that was enforced by a retaining wall such that a stagnant heap was formed that is growing in mass as long as it is fed from the upstream end by a continuous flow of material. Video films and CCD photographs were made. They allow exact determination in the experiment of the following:

(i) the evolution of the geometry of the heap from its inception to its final form;
(ii) the velocity distribution including its transition from the supercritical state in the upstream regime via the diffusive jump with the transition from the supercritical to the subcritical regime, and eventually standstill;
(iii) the speed of the tip of the diffusive shock and the local geometry of the shock structure;
(iv) the velocity distribution, including its boundary layer structure within the shock region and its attenuation to an apparent standstill far below the free surface of the heap; and
(v) the transition of the basically uniform distribution of the supercritical velocity in the thin upstream layer to the nonuniform boundary layer flow within the shock regime, etc.

Various kinematic quantities were determined from the photographs taken by the video and CCD cameras and the data obtained by using PIV measurements: maximum and impact velocities at the transition point from the supercritical to the subcritical flow were determined as were flow height and momentum flux. The most significant variables are the shock speed and the flow height. A single mass balance relation at the shock discontinuity corroborated the correlation existing between the shock height and shock speed, in good agreement with the experiments.

This report only provides the first steps in the exploitation of the detailed experiments. To clearly identify the above steps, further analysis with the recorded data is needed. The information gained by such work will, however, be significant. Most granular avalanche flows into the deposition region are typically characterized by transitions from supercritical states via a shock to a standstill. A proper model ought to be able to describe such transitions not only qualitatively, but also quantitatively. The next steps must therefore consist of the development of the mathematical model that reproduces the shock and mentioned transitions from supercritical uniform flow in the upstream regime to a boundary layer flow in the diffusive shock to standstill in the stagnant heap. Once solved, the analogous problem without retaining wall can be attacked to properly describe the flow into the deposition zone. And at last the corresponding three-dimensional motion of a granular avalanche into the deposition could be attacked.

There is, however, also a further application of these experiments: They may provide detailed information of the

flow characteristics when an obstructing wall is hit by a layer of rapidly moving grains. A clear understanding of this type of flow, in particular with regard to the mechanism of tractions exerted by the granular material on the obstructing walls is urgently needed, since depth integrated models do not provide us with satisfactory answers.

The above discussion should make it clear that the reported experiments comprise a first, important step in acquiring a better and more detailed understanding of the transition mechanism of rapid granular flows into a zone of relative standstill. Its solution will provide a better understanding both of the mass distribution in such zones as well as force flows to the boundaries of such regimes.

ACKNOWLEDGMENTS

The chute was built by the workshop personnel H. Hoffmann, H. Wiener, and C. Bonk of the Department of Mechanics, Darmstadt University of Technology. Their efforts are gratefully acknowledged. The financial support was provided by *Deutscher Akademischer Austauschdienst (DAAD)* (German Academic Exchange Service), and National Science Council, Taiwan, for the years 2004/05 through the *Project-Based Personal Exchange Program*. We acknowledge Hsiang-Jen Cheng from NCU, Chung-Li for his help in the experiments. We would like to thank the reviewers for the constructive criticisms which helped to improve the quality of the paper.

[1] S. B. Savage and K. Hutter, "The motion of a finite mass of granular material down a rough incline," J. Fluid Mech. **199**, 177 (1989).
[2] S. B. Savage and K. Hutter, "Dynamics of avalanches of granular materials from initiation to runout. Part I, Analysis," Acta Mech. **86**, 201 (1991).
[3] J. M. N. T. Gray, M. Wieland, and K. Hutter, "Gravity-driven free surface flow of granular avalanches over complex basal topography," Proc. R. Soc. London, Ser. A **455**, 1841 (1999).
[4] S. P. Pudasaini, "Dynamics of flow avalanches over curved and twisted channels, theory, numerics and experimental validation," Ph.D. dissertation, Darmstadt University of Technology, Germany (2003).
[5] S. P. Pudasaini and K. Hutter, "Rapid shear flows of dry granular masses down curved and twisted channels," J. Fluid Mech. **495**, 193 (2003).
[6] S. P. Pudasaini and K. Hutter, *Avalanche Dynamics: Dynamics of Rapid Flows of Dense Granular Avalanches* (Springer Verlag, Berlin, 2006).
[7] S. P. Pudasaini, Y. Wang, and K. Hutter, "Rapid motions of free-surface avalanches down curved and twisted channels and their numerical simulation," Philos. Trans. R. Soc. London, Ser. A **363**, 1551 (2005).
[8] S. P. Pudasaini, Y. Wang, and K. Hutter, "Modelling debris flows down general channels," Nat. Hazards Earth Syst. Sci. **5** (2005).
[9] S. P. Pudasaini, S.-S. Hsiau, Y. Wang, and K. Hutter, "Velocity measurements in dry granular avalanches using particle image velocimetry technique and comparison with theoretical predictions," Phys. Fluids **17**, 093301 (2005).
[10] Y. Wang, K. Hutter, and S. P. Pudasaini, "The Savage-Hutter theory: A system of partial differential equations for avalanche flows of snow, debris and mud," ZAMM **84**, 507 (2004).
[11] K. Hutter, Y. Wang, and S. P. Pudasaini, "The Savage-Hutter avalanche model. How far can it be pushed?" Philos. Trans. R. Soc. London, Ser. A **363**, 1507 (2005).
[12] R. P. Denlinger and R. M. Iverson, "Granular avalanches across irregular three-dimensional terrain, 1. Theory and computation," J. Geophys. Res. **109** (2004).
[13] R. M. Iverson, M. Logan, and R. P. Denlinger, "Granular avalanches across irregular three-dimensional terrain, 2. Experimental tests," J. Geophys. Res. **109** (2004).
[14] A. K. Patra, A. C. Bauer, C. C. Nichita, E. B. Pitman, M. F. Sheridan, M. Bursik, B. Rupp, A. Weber, A. Stinto, L. Namikawa, and C. Renschler, "Parallel adaptive numerical simulation of day avalanches over natural terrain," J. Volcanol. Geotherm. Res. **139**, 1 (2005).
[15] E. B. Pitman, C. C. Nichita, A. K. Patra, A. C. Bauer, M. Bursik, and A. Weber, "A numerical study of granular flows on erodible surface," Discrete Contin. Dyn. Syst., Ser. B **3**, 589 (2003).
[16] W. Eckart, N. Gray, and K. Hutter, "Particle image velocimetry (PIV) for granular avalanches on inclined planes," in *Lecture Notes in Applied and Computational Mechanics—LNACM*, edited by K. Hutter and N. Kirchner (Springer Verlag, Berlin, 2003), Vol. 11.
[17] M. Tischer, M. I. Bursik, and E. B. Pitman, "Kinematics of sand avalanches using particle image Velocimetry," J. Sediment Res. **71**, 355 (2001).
[18] See EPAPS Document No. E-PHFLE6-19-026704 for data files for velocity fields measured by using PIV system for rapid granular flows and other associated plots. This document can be reached via a direct link in the online article's HTML reference section or via the EPAPS homepage (http://www.aip.org/pubservs/epaps.html).